Fatigue of concrete studied using a confined punch-through shear test

Mario Aguilar, Henrik Becks, Abedulgader Baktheer, Martin Classen, Rostislav Chudoba

Lehrstuhl und Institut für Massivbau,
RWTH Aachen University,
Mies-van-der-Rohe-Straße 1, 52074 Aachen, Germany

E-Mail: maguilar@imb.rwth-aachen.de

Abstract

Accurate prediction of fatigue in reinforced concrete structures remains a challenging goal that is receiving increasing attention in research. Understanding concrete fatigue is critical as future infrastructures will need to be built with less concrete for environmental reasons while requiring longer service life. We present a physically based modeling approach in which fatigue-induced degradation is linked to inter-aggregate shear strain. The paper presents a summary of the microplane model MS1, which includes this fatigue mechanism at the microplane-interface level. To validate fatigue life predictions of the model, the authors performed standard cylinder compression tests in which the failure mechanism is due to shear bands occurring in the latter stages of the fatigue life. A non-controllable and not easily quantifiable combination of shear and compressive stress prevails in the localized material zone. To better understand and isolate these mechanisms, the authors developed a modified version of the punch-through shear test, which permits precise simultaneous and independent application of shear and compressive loading. Experimental and numerical simulations of the PTST response under different levels of confinement are presented for the monotonic and fatigue behavior of the tests. Finally, the energy dissipation of the PTST under two different levels of confinement is quantified for cyclic loading.

Keywords: fatigue, material modelling, experimental characterization, mode II loading

Kurzfassung

Die genaue Vorhersage der Ermüdung von Stahlbetonbauteilen ist nach wie vor ein anspruchsvolles Ziel, das in der Forschung zunehmend an Aufmerksamkeit gewinnt. Das grundlegende Verständnis der reinen Betonermüdung ist hierbei von entscheidender Bedeutung, da künftige Infrastrukturbauwerke der Umwelt zuliebe mit weniger Beton gebaut werden müssen und gleichzeitig eine längere Lebensdauer erfordern. In unserem Beitrag stellen wir einen physikalisch-basierten Modellierungsansatz vor, in dem die ermüdungsbedingte Degradation mit der Schubdehnung zwischen den Zuschlagskörnern verknüpft ist. Die Veröffentlichung enthält eine Zusammenfassung des Microplane-Models MS1, das diesen Ermüdungsmechanismus auf der Ebene der Microplane beinhaltet. Zur Validierung der Modellvorhersagen zur Ermüdungslebensdauer führten die Autoren zylindrische Standard-Druckversuche durch, bei denen der Versagensmechanismus auf schubinduzierte Gleitbrüche zurückzuführen ist, die in den letzten Phasen der Ermüdungslebensdauer auftreten. In der lokalisierten Materialzone herrscht eine nicht steuerbare und nicht leicht quantifizierbare Kombination aus Schub- und Druckspannungen. Um diese Mechanismen besser zu verstehen und zu isolieren, entwickelten die Autoren eine modifizierte Version des Punch-Through Shear Test (PTST), die eine präzise gleichzeitige und unabhängige Anwendung von Scher- und Druckbelastungen ermöglicht. Experimentelle und numerische Simulationen der PTST mit verschiedenen Niveaus der seitlichen Druckbeanspruchung werden für das monotone und das Ermüdungsverhalten der Tests vorgestellt. Schließlich wird die Energiedissipation des PTST bei zyklischer Belastung unter zwei verschiedenen seitlichen Druckbeanspruchungsniveaus quantifiziert.

Keywords: Ermüdung, Materialmodellierung, experimentelle Charakterisierung, Mode-II Belastung

1 Introduction

Predicting the fatigue life of concrete structures is a challenging task that is increasingly gaining attention from researchers. To tackle the upcoming environmental challenges, it is crucial to have a more profound comprehension of concrete fatigue. These challenges require finding a way to balance the high carbon footprint of the concrete construction industry with an increasing global demand. As a result, future infrastructure must use less concrete while prolonging the service life of current and future structures. A comprehensive description of fatigue phenomena covering both material and structural levels is required for this transformative shift.

In recent research, a dissipation hypothesis has been introduced by the authors, attributing the primary fatigue-induced degradation mechanism to the cumulative inter-aggregate shear strain. This hypothesis results in a new formulation of a pressure-sensitive interface model that is applicable to both discrete models and tensorial microplane models. Realistic modeling of fatigue behavior in cementitious interfaces [1], concrete subjected to compressive fatigue loading [2], and fatigue shear behavior of confined concrete [3, 4] has been accomplished using this hypothesis.

2 Punch-through shear test

The cylindrical punch-through shear test (PTST) was originally introduced by Luong et al. [5] to study concrete and rock behavior under combined shear and compression loads. Building on this, Backers et al. [6] adapted the test to assess rock fracture toughness in mode II. Recent research has extended the application of the PTST to explore concrete fatigue [7], revealing how compressive stress significantly affects fatigue life during Mode II loading.

One of the main advantages of the PTST lies in its predefined fracture surface, ensuring consistent stress configuration across all fatigue stages and test series, enhancing reproducibility. In contrast, conventional cylinder tests used to characterize compressive fatigue behavior of concrete assume a uniaxial stress state during initial stages. As fatigue progresses to stage III, distinct shear bands form, influenced by the friction between load plates and cylinder surfaces, varying in number, position and inclination within test series. In stage III, the localized shear bands create an a priori unknown combined compression and shear stress state. This transition from uniaxial to multi-axial stress state, as numerically evaluated in [4], significantly impacts the remaining fatigue life, contributing to a wide scatter in the observed fatigue life, typically spanning orders of magnitude [2].

To validate the fatigue hypotheses under different loading conditions, a test setup that allows the adjustment of the normal and shear loads within a material zone seems appealing. Since there is no standardized test for studying the confined shear behavior of concrete, the authors have presented a refined version of the PTST [7, 8].

This enhanced PTST setup permits simultaneous and independent application of shear and compressive loading, enabling focused study of the impact of the confinement on the fatigue life of concrete under subcritical fatigue shear loading [8]. The refined setup reduces scatter in measured fatigue life, achieving consistent failure surfaces for all specimens, as the one shown in Fig. 1. This diminished scatter allows for investigating the load sequence effect, crucial for accurate estimation of structural concrete fatigue life.

3 Microplane fatigue model MS1

The experimental results of the PTST from [7, 8] are analyzed using the recently developed material model MS1 [2, 9–11]. The MS1 model relates the macroscopic fatigue damage to the local cumulative inelastic shear strain at the microplane level. This allows for the reproduction of the tri-axial stress redistribution that occurs within the material structure under pulsating subcritical loading. This hypothesis is consistent with experimental observations by Skarzynski et al. [12], where fatigue-related crack initiation and propagation under compressive fatigue loading mainly occur along the interfaces between hardened cement paste and aggregates, as shown in Fig. 2. The model is formulated within the microplane framework and utilizes the kinematic constraint to project the macroscopic strain tensor onto the microplanes. To homogenize microplane stresses, secant, and plastic strain tensors, the model employs the principle of virtual work and energy equivalence.

DOI: 10.18154/RWTH-2023-06653

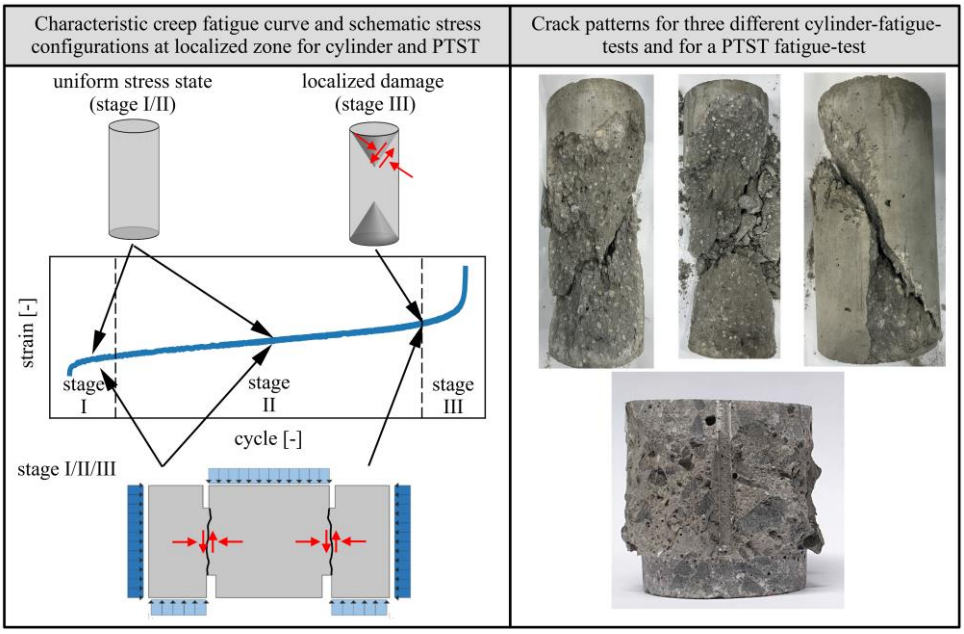

Figure 1 On the left: a typical creep fatigue curve of concrete with schematic characteristic fracture surface and stress configuration for cylinders and PTSTs. On the right: experimental fracture surfaces of three different cylinder tests and a PTST [8] after fatigue loading.

3.1 Thermodynamically based formulation and evaluation of energy dissipation

Thermodynamically-based constitutive laws are utilized to capture distinct degradation mechanisms at the microplane level, representing the inter-aggregate material behavior within a 3D material structure in a specific direction. The macroscopic Helmholtz free energy is obtained as the integral of the sum of the microplane normal and tangential thermodynamic potentials.

$$\psi^{\mathrm{mac}} = \frac{3}{2\pi}\int_{\Omega} \psi^{\mathrm{mic}} d\Omega = \frac{3}{2\pi}\int_{\Omega} \psi_{\mathrm{N}}\, d\Omega + \frac{3}{2\pi}\int_{\Omega} \psi_{\mathrm{T}}\, d\Omega \tag{1}$$

The distinction between normal and tangential thermodynamic potentials allows to assign distinguished dissipative mechanisms for each direction, covering the anisotropic and heterogeneous nature of concrete in a simple and realistic manner. In the microplane model MS1, the primary cause of fatigue damage is considered to be the cumulative inter-aggregate relative displacements. In order to reflect this hypothesis at the microplane level, the fatigue damage evolution in the tangential direction is related to the cumulative sliding, following [13]. To account for the inter-aggregate interaction in the normal direction, simple damage is considered for the tensile behavior and hardening plasticity for the compressive behavior. Fig. 2 provides a schematic overview of these dissipative mechanisms. The formulation of the Helmholtz free energy functions ψ_{N} and ψ_{T} of a microplane is expressed as follows:

$$\rho\psi_{\mathrm{N}}^{\mathrm{mic}} = \frac{1}{2}(1 - H(\sigma_{\mathrm{N}})\omega_{\mathrm{N}})E_{\mathrm{N}}\left(\varepsilon_{\mathrm{N}} - \varepsilon_{\mathrm{N}}^{\mathrm{p}}\right)^2 + \frac{1}{2}K_{\mathrm{N}}z_{\mathrm{N}}^2 + \frac{1}{2}\gamma_{\mathrm{N}}{\alpha_{\mathrm{N}}}^2 \tag{2}$$

$$\rho\psi_{\mathrm{T}}^{\mathrm{mic}} = \frac{1}{2}(1 - \omega_{\mathrm{T}})E_{\mathrm{T}}(\boldsymbol{\varepsilon_{\mathrm{T}}} - \boldsymbol{\varepsilon_{\mathrm{T}}^{\pi}}) \cdot (\boldsymbol{\varepsilon_{\mathrm{T}}} - \boldsymbol{\varepsilon_{\mathrm{T}}^{\pi}}) + \frac{1}{2}K_{\mathrm{T}}z_{\mathrm{T}}^2 + \frac{1}{2}\gamma_{\mathrm{T}}\boldsymbol{\alpha_{\mathrm{T}}} \cdot \boldsymbol{\alpha_{\mathrm{T}}} \tag{3}$$

Where E_{N} and E_{T} are the normal and tangential elastic stiffness, defined as $E_{\mathrm{N}} = E/(1-2\nu)$, $E_{\mathrm{T}} = E(1-4\nu)/((1+\nu)(1-2\nu))$. K_{N},γ_{N},K_{T} and γ_{T} represent the normal and tangential isotropic and kinematic strain hardening moduli, respectively. The thermodynamic state variables consist of the normal and tangential plastic strain $\varepsilon_{\mathrm{N}}^{\mathrm{p}}$ and $\boldsymbol{\varepsilon_{\mathrm{T}}^{\pi}}$, the normal and tangential damage ω_{N} and ω_{T}, the normal and tangential isotropic hardening variables z_{N} and z_{T} , and the normal and tangential kinematic hardening variables α_{N} and α_{T}.

DOI: 10.18154/RWTH-2023-06653

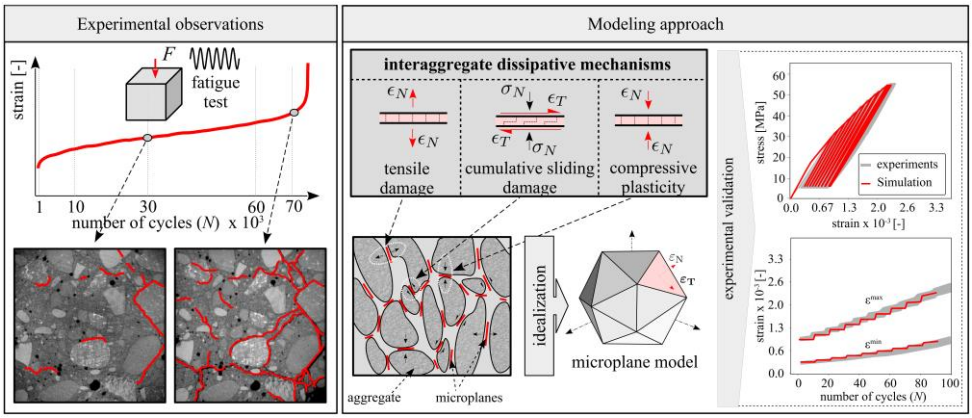

Figure 2 left: experimental observations of microcrack development under compressive fatigue loading using X-ray micro-CT images obtained by Skarzynski et al. [12]. Center: schematic interaggregate dissipative mechanisms included in MS1 and illustration of the microstructure containing a system of dissipative microplanes. Right: schematic experimental validation procedure presented in [2].

The conjugate thermodynamic forces for the normal and tangential direction are obtained by differentiating the corresponding thermodynamic potential with respect to the associated state variable. For a detailed model description, including the definition of the normal and tangential governing threshold functions and the evolution laws, see [2]. Additionally, Fig. 2 provides a schematic overview of the material model, illustrating the calibration-validation procedure used at [2].
The evaluation of energy dissipation for an isothermal process, assuming small strains, is described by the Clausius-Duhem inequality. In the normal direction it is given as $\dot{D}_{\mathrm{int}}^{\mathrm{N}} = -\rho\dot{\psi}_{\mathrm{N}} + \sigma_{\mathrm{N}}\dot{\epsilon}_{\mathrm{N}} \geq 0$. To obtain the overall energy dissipation related to a microplane in the normal direction, $\dot{\psi}_{\mathrm{N}}$ is substituted by differentiating Eq. 2, by applying the chain rule, as detailed in [14]. Then, by integrating the dissipation rates over the pseudo-time t, this procedure results in the following expression:

$$D_{\mathrm{int}}^{\mathrm{N}} = \int_0^t [\sigma_{\mathrm{N}}\dot{\epsilon}_{\mathrm{N}}^{p} - Z_{\mathrm{N}}\dot{z}_{\mathrm{N}} - X_{\mathrm{N}}\dot{\alpha}_{\mathrm{N}} + Y_{\mathrm{N}}\dot{\omega}_{\mathrm{N}}] \geq 0. \tag{4}$$

Analogously, Clausius-Duhem inequality for the tangential direction is expressed as $\dot{D}_{\mathrm{int}}^{\mathrm{T}} = -\rho\dot{\psi}_{\mathrm{T}} + \boldsymbol{\sigma}_{\mathbf{T}} \cdot \dot{\boldsymbol{\epsilon}}_{\mathbf{T}} \geq 0$. After operating as for the normal direction, the total energy dissipation for the tangential direction can be expressed as:

$$D_{\mathrm{int}}^{\mathrm{T}} = \int_0^t [\boldsymbol{\sigma}_{\mathbf{T}} \cdot \dot{\boldsymbol{\epsilon}}_{\mathbf{T}}^{\boldsymbol{\pi}} - Z_{\mathrm{T}}\dot{z}_{\mathrm{T}} - \boldsymbol{X}_{\mathbf{T}} \cdot \dot{\boldsymbol{\alpha}}_{\mathbf{T}} + Y_{\mathrm{T}}\dot{\omega}_{\mathrm{T}}] \geq 0. \tag{5}$$

By integrating the energy dissipation for each microplane, the macroscopic energy dissipation can be obtained as:

$$D_{\mathrm{int}}^{\mathrm{mac}} = \frac{3}{2\pi}\int_{\Omega} D_{\mathrm{int}}^{\mathrm{mic}}\, d\Omega = \frac{3}{2\pi}\int_{\Omega} D_{\mathrm{int}}^{\mathrm{N}}\, d\Omega + \frac{3}{2\pi}\int_{\Omega} D_{\mathrm{int}}^{\mathrm{T}}\, d\Omega \tag{6}$$

4 Numerical results

4.1 Monotonic behavior

In order to assess how the microplane material model MS1 performs in reproducing PTST behavior under varying degrees of normal confinement, a study using Mode II displacement control loading is presented in Fig. 3. The parameters of the model were adjusted to match the monotonic experimental strength of the material of the first test series presented at [8], where five levels of confinement were studied: 0, 4, 8, 16, and 32 MPa.

The force-displacement curves, obtained numerically for the five studied cases are shown in the upper left panel of Fig. 3. In particular, both peak load and stiffness -to a lesser extent- show an increase with increasing confinement. The corresponding experimental monotonic behavior is shown in the top

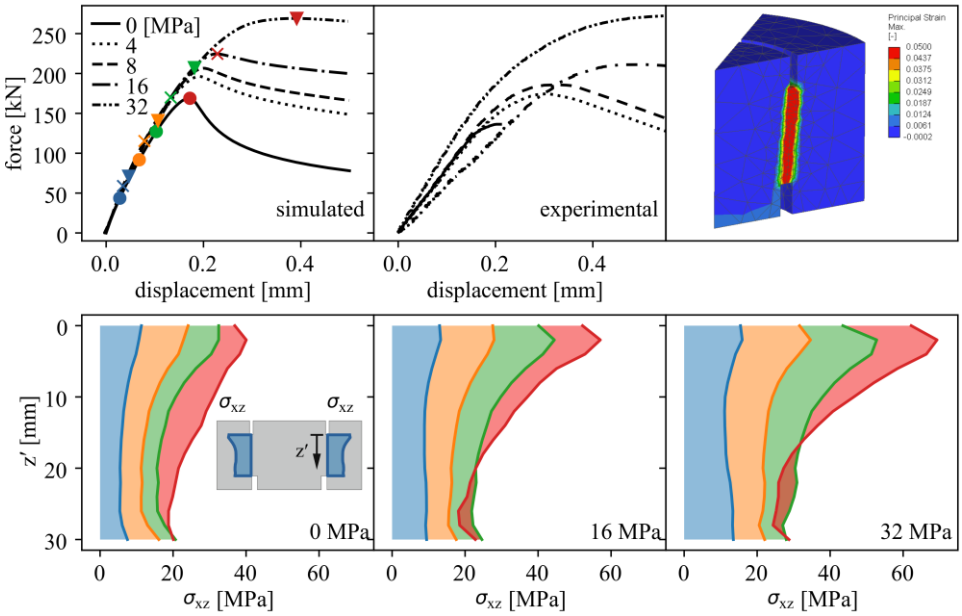

Figure 3 Top left and middle figures correspond to the simulated and experimental [8] monotonic behavior for the PTST, respectively. The top left panel displays the failure surface for experimental and simulated results. The bottom row shows the shear stress distribution σ_{xz} along the ligament height for 25% (blue), 50% (orange), 75% (green) and 100% (red) of the peak load for the indicated confinement level. Material parameters: $E = 39226$, $\nu = 0.18$, $\varepsilon_N^0 = 1e^{-5}$, $A_d = 7000$, $\sigma_N^0 = 40$, $\gamma_N = 80000$, $K_N = 14000$, $\sigma_T^0 = 10$, $\gamma_T = 120000$, $K_T = 1200$, $S_T = 0.01$, $r_T = 8.5$, $c_T = 7.5$, $p_T = 7.5$, $m_T = 0.05$.

middle panel of Fig. 3. Numerical and experimental peak loads are in good agreement for each level of confinement.

The numerical model discretization and corresponding fracture surface in terms of ε_I are illustrated in the top right of Fig. 3. Shear stress σ_{xz} profiles along the PTST ligament are depicted in the bottom row. σ_{xz} is averaged over the ligament thickness and plotted against the height. This is done in a local coordinate system outlined in the lower left panel. Shear stresses are evaluated at four points on the load-displacement curves: -25% in blue, 50% in orange, 75% in green, and 100% in red of the peak load with confinement levels of 0, 16, and 32 MPa. Relatively uniform shear stress profiles can be observed at 25% of the peak load. As the load level increases, the shear stress at the upper part of the ligament exhibits an upward trend, particularly at higher confinements. This phenomenon results from two radial effects. The first is a greater quasi-uniform confinement influence, and the second is bending due to the vertical load. These effects combine to compress the upper part of the ligament, where higher confinement joins increased compressive stress from the bending under higher peak loads. Consequently, the shear strength of the upper part of the ligament significantly increases because the material is pressure-sensitive. On the other hand, the lower part of the ligament undergoes a partial offset; higher confinement is counteracted by superimposed tensile stress from bending under increased peak load.

While shear stress profiles may lack uniformity, the primary advantage of the test setup is its ability to control lateral and vertical loading and the fracture surface. The resultant stress profile is numerically determinable since it depends solely on the applied loads and specimen geometry. This differs from cylinder tests, where failure surfaces can vary from test to test, resulting in different stress configurations.

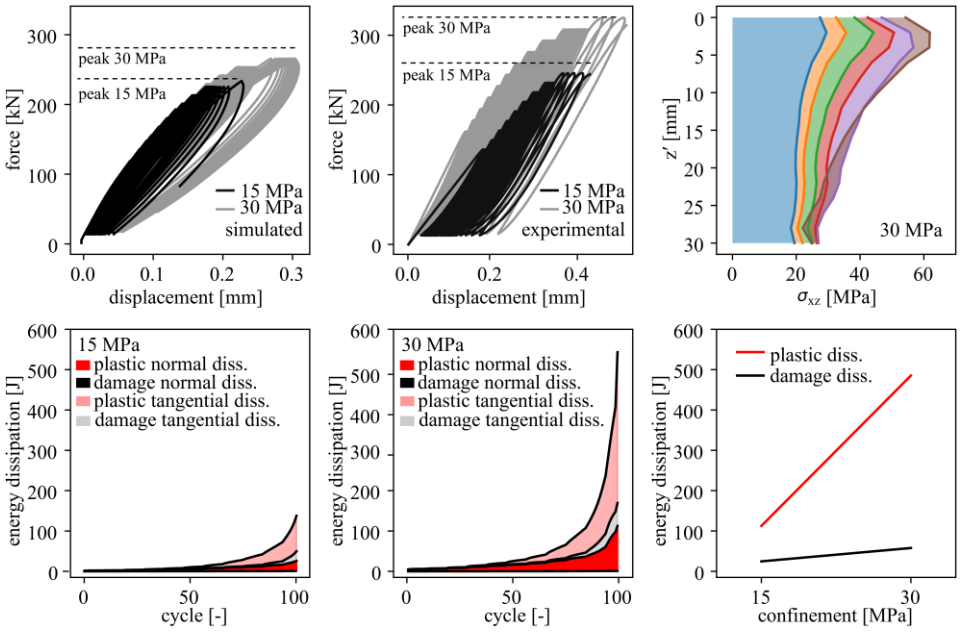

Figure 4 Top left and middle figures correspond to the simulated and experimental [8] step-wise increasing cyclic behavior for the PTST, respectively. Top right panel displays the shear stress distribution σ_{xz} along the ligament height for 50 (blue), 60 (orange), 70 (green), 80 (red), 90 (purple) and 95% (brown) for a confinement level of 30 MPa. Bottom left and middle figures correspond to the cumulative energy dissipation associated with each dissipative mechanism along the cycles for the case of 15 and 30 MPa confinement levels, respectively. The lower right figure shows the accumulated energy dissipation for each confinement level due to damage and plasticity. Material parameters as specified in the caption of Fig. 3

4.2 Fatigue behavior

The ability of the model to reproduce the response of confined concrete under cyclic subcritical shear loading was evaluated using a loading scenario with incremental upper load levels. Cyclic loading consisted of 10 cycles at each load level. The tests started with a maximum shear load of $S_{\max} = 0.5$ and increased gradually by $\Delta S_{\max} = 0.5$. The lower load level remained constant at $S_{\min} = 0.05$. This loading scenario offers the possibility to rapidly and effectively characterize the fatigue behavior of concrete for various loading amplitudes.

The force-displacement response under this loading scheme for confinement levels of 15 and 30 MPa is simulated and illustrated in the top-left of Fig. 4. The predictions are based on material parameters from the previous monotonic study, illustrated in Fig. 3, that are calibrated using the first test series from [8]. Although a quantitative prediction-measurement comparison is not possible due to the lack of an analogous cyclic loading scenario on the same batch of specimens, qualitative insights can be gained. The results for this loading scheme from the second test series in [8] are presented in the top middle panel, showing higher peak load value, as indicated by the dashed lines.

The current calibration enables the qualitative analysis of stress distribution at the ligament for various loading amplitudes, as shown in Fig. 4 top right panel. Shear stress profiles are obtained in a similar manner to Fig. 3, for the 30 MPa confinement level for 50%, 60%, 70%, 80%, 90%, and 95% of the maximum peak load. The breakdown of energy dissipation is illustrated in the bottom row. The cumulative energy dissipation related to each dissipative mechanism is presented in the left and middle figures for confinement levels of 15 and 30 MPa, respectively. The figure on the lower right depicts the accumulated energy dissipation for each confinement level due to damage and plasticity, without

distinguishing between normal and tangential directions. Remarkably, the plastic energy dissipation increases significantly, whereas damage energy dissipation remains relatively stable. Previous numerical studies by the authors [4, 14] consistently yielded similar results. These studies indicated that the damage energy dissipation doesn't change as dramatically as the plastic energy dissipation for simulations of the same test setup under identical boundary conditions.

5 Conclusions

The fatigue behavior of confined concrete under shear fatigue loading was investigated using a newly developed version of PTST. This innovative setup provides independent control of confinement level and shear loading. Furthermore, all tested specimens had the same fracture surface, resulting in a consistent stress configuration in the localized zone over both the fatigue life and the test series. In contrast, the standard cylinder test induces a uniform uniaxial compressive stress, which is mainly valid during the early stages of the fatigue life (stages I and II) in the fatigue creep curve. During stage III, as damage localizes into a shear band, a non-uniform and undefined combination of compressive and shear stress occurs due to factors like crack position, inclination, and number, which is in turn influenced by cylinder-plate friction.

The PTST allows for systematic study of concrete fatigue under combined compressive and shear loading. This paper presents experimental results on confined monotonic and subcritical cyclic shear behavior. The results have been qualitatively replicated using the MS1 model with finite element analysis. The microplane-level pressure-sensitive interface formulation used in MS1 reproduces increased shear strength with higher confinement in a manner that reflects the experimentally observed peak load rise. Additionally, MS1 captures damage propagation under subcritical pulsating loading, including an accelerated damage evolution for higher loading amplitudes that qualitatively agrees with the Wöhler (S-N) curves of concrete. The thermodynamic formulation used in MS1 allows the evaluation of energy dissipation for each dissipative mechanism. These studies have unveiled significant variations in plastic energy dissipation per loading scenario, while damage dissipation remains relatively consistent. These insights serve as a foundation for making more realistic fatigue life predictions in concrete structures.

Aknowledgments

The authors gratefully acknowledge the support for this research by the German Research Foundation (Deutsche Forschungsgemeinschaft DFG), in (I) the scope of the Priority Program SPP2020 "Cyclic deterioration of high-performance concrete in an experimental virtual lab", (Project number: 441550460), (II) the scope of the joint project "Energy dissipation-based approach to stochastic fatigue of concrete considering interacting time and temperature effects", Project number: 471796896).

References

[1] Chudoba, R.; Vořechovský, M.; Aguilar, M. et al.: Coupled sliding–decohesion–compression model for a consistent description of monotonic and fatigue behavior of material interfaces. In: Computer Methods in Applied Mechanics and Engineering 398 (2022), S. 115259. https://doi.org/10.1016/j.cma.2022.115259.

[2] Baktheer, A.; Aguilar, M.; Chudoba, R.: Microplane fatigue model MS1 for plain concrete under compression with damage evolution driven by cumulative inelastic shear strain. In: International Journal of Plasticity, Vol. 143 (2021). https://doi.org/10.1016/j.ijplas.2021.102950.

[3] Aguilar, M.; Baktheer, A.; Chudoba, R.: On the energy dissipation in confined concrete subjected to shear cyclic loading. In: Proceedings in Applied Mathematics and Mechanics (PAMM), Vol. 22 (2023). https://doi.org/10.1002/pamm.202200301.

[4] Aguilar, M.; Baktheer, A.; Becks, H. et al.: Fatigue-induced concrete fracture under combined compression and shear studied using standard cylinder and refined punch-through shear test setup. In: Proceedings of the 11th International Conference on Fracture Mechanics of Concrete and Concrete Structures.

[5] Luong, M.P.: Fracture behaviour of concrete and rock under mode II and mode III shear loading. In: Shah, S.P.; Swartz, S.E.; Barr, B. (eds.): Fracture of Concrete and Rock – Recent developments. Elsevier Applied Science, Cardiff, United Kingdom, 1989, pp. 18-26.

[6] Backers, T.; Stephansson, O.; Rybacki, E.: Rock fracture toughness testing in Mode II—punch-through shear test. In: International Journal of Rock Mechanics and Mining Sciences, Vol. 39 (2002), Iss. 6, pp. 755-769. https://doi.org/10.1016/S1365-1609(02)00066-7.

[7] Becks, H.; Classen, M.: Mode II Behavior of High-Strength Concrete under Monotonic, Cyclic and Fatigue Loading. In: Materials, Vol. 14 (2021), Iss. 24, 7675. https://doi.org/10.3390/ma14247675.

[8] Becks, H.; Aguilar, M.; Chudoba, R. et al.: Characterization of high-strength concrete under monotonic and fatigue mode II loading with actively controlled level of lateral compression. In: Materials and Structures, Vol. 55 (2022), Iss. 252. https://doi.org/10.1617/s11527-022-02087-4.

[9] Baktheer, A.; Aguilar, M.; Hegger, J. et al.: Microplane damage plastic model for plain concrete subjected to compressive fatigue loading. In: Pijaudier-Cabot, G.; Grassl. P.; La Borderie, C. (eds.): Proceedings of the 10th International Conference on Fracture Mechanics of Concrete and Concrete Structures, Bayonne, France, 2019.

[10] Becks, H.; Aguilar, M.; Baktheer, A. et al.: Experimental and numerical investigations on the fatigue behavior of high-strength concrete under combined shear-compression loading. In: IABSE (ed.): Proceedings of IABSE Symposium: Challenges for Existing and Oncoming Structures. IABSE, Prague, Czech Republic, 2022, 532–540.

[11] Becks, H.; Aguilar, M.; Hegger, J. et al.: Experimental and Numerical Characterization of High-Strength Concrete Under Monotonic and Fatigue Mode II Loading with Active Control of Lateral Compression. In: Fédération internationale du béton (ed.): Building for the future: Durable, Sustainable, Resilient – Proceedings of the fib Symposium 2023. International Federation for Structural Concrete, Digital Proceedings, Istanbul, Turkey, 2023, pp. 429-439.

[12] Skarżyński, Ł.; Marzec, I.; Tejchman, J.: Fracture evolution in concrete compressive fatigue experiments based on X-ray micro-CT images. In: International Journal of Fatigue, Vol. 122 (2019), pp. 256-272. https://doi.org/10.1016/j.ijfatigue.2019.02.002.

[13] Baktheer, A.; Chudoba, R.: Pressure-sensitive bond fatigue model with damage evolution driven by cumulative slip: Thermodynamic formulation and applications to steel- and FRP-concrete bond. In: International Journal of Fatigue, Vol. 113 (2018), pp. 277-289. https://doi.org/10.1016/j.ijfatigue.2018.04.020.

[14] Aguilar, M.; Baktheer, A.; Chudoba, R.: Numerical investigation of load sequence effect and energy dissipation in concrete due to compressive fatigue loading using the new microplane fatigue model MS1. In: Oñate, E.; Perić, D.; Chiumenti, M. et al. (eds.): Proceedings of the 16th International Conference on Computational Plasticity, Barcelona, Spain, 2021, pp. 1-12.